

# Measuring the Effective Young's Modulus of Structural Silicone Sealant in Moment-Resisting Glazing Joints

Adam D. Lee<sup>a,b,\*</sup>, Paul Shepherd<sup>a</sup>, Mark C. Evernden<sup>a</sup>, David Metcalfe<sup>c</sup>

<sup>a</sup>*Department of Architecture and Civil Engineering, University of Bath, Claverton Down, Bath, BA2 7AY, U.K.*

<sup>b</sup>*PTCC Facade Design, Telecom Plaza, 316 Senator Gil Puyat Ave., Makati City, Metro Manila, 1200, Philippines.*

<sup>c</sup>*Centre for Window and Cladding Technology (CWCT), The Studio, Entry Hill, Bath, BA2 5LY, U.K.*

---

## Abstract

Structural silicone sealants are synthetic rubber adhesives used in the construction industry to bond glass and other sheet infill materials to the frames of windows and curtain walls. In this paper, two different algebraic expressions are proposed to describe the way in which the rotational stiffness of the adhesive connection – resistance to moments acting about the axis of the joint – varies with the sealant's cross-sectional dimensions and elastic modulus. Laboratory testing of DC-983, a two-component structural silicone sealant used widely in factory prefabricated glazing applications, has, with some caveats, validated the mathematical models.

*Keywords:* facade design, structural silicone sealant, structural glazing, elastic modulus, curtain wall, mullion,

---

## 1. Introduction

1                    In the middle of last century there began to emerge, hand in hand with  
2                    the glass box architectural style, a new method of constructing tall buildings.  
3                    First, a frame made up of columns and beams was erected, to support the  
4                   

---

\*Corresponding Author

*Email addresses:* [adamlee@torstencalvi.com](mailto:adamlee@torstencalvi.com) (Adam D. Lee), [p.shepherd@bath.ac.uk](mailto:p.shepherd@bath.ac.uk) (Paul Shepherd), [m.evernden@bath.ac.uk](mailto:m.evernden@bath.ac.uk) (Mark C. Evernden), [david.metcalfe@cwct.co.uk](mailto:david.metcalfe@cwct.co.uk) (David Metcalfe)

*Preprint submitted to Elsevier "Construction & Building Materials"*

*May 25, 2018*

<http://dx.doi.org/10.1016/j.conbuildmat.2018.06.038>

© 2018. This manuscript version is made available under the CC-BY-NC-ND 4.0 license

<http://creativecommons.org/licenses/by-nc-nd/4.0/>

5 floors; then, to keep out the weather, the freestanding structure was enclosed  
 6 with a lightweight, metal framed, skin [1, 2, 3]. Since that time, designers of  
 7 these exterior “curtain walls” have been using the same set of assumptions when  
 8 modelling the forces that are transferred from the sheet material covering the  
 9 facade, which is often glass, to the members in the supporting frame. These  
 10 structural idealizations are illustrated in Figure 1, in four cross-sections through  
 11 extruded aluminium “mullion” profiles, which are those that span vertically from  
 12 one floor to another.

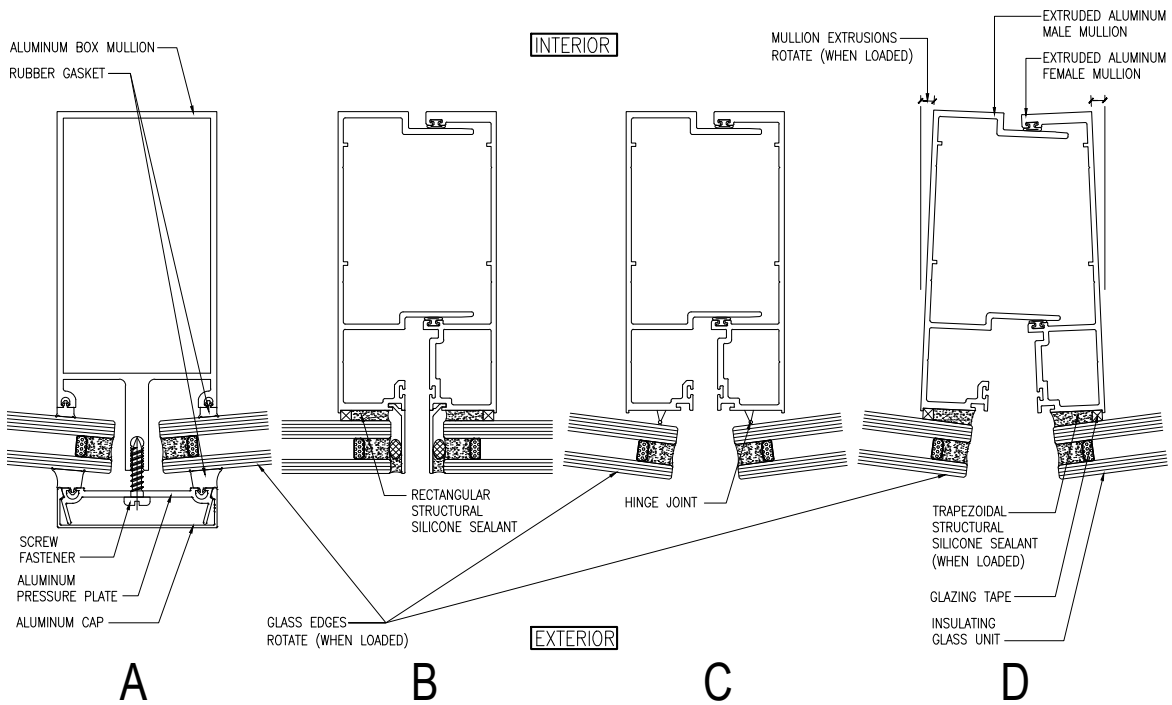


Figure 1: Cross-sectional shapes of vertical mullions. In detail “A”, glass is held mechanically to a simple box section. Structural sealant, in detail “B”, bonds glass to the male and female profiles of a unitized wall’s split mullion: this design’s structural idealization is shown in “C”, although “D” may be a better represent the wall’s actual behaviour when subjected to wind load.

13 The first of the mullions, Figure 1-A, is a simple box section. Aluminium  
 14 curtain wall profiles of this sort, which must be cut and assembled at the construction site, became popular in the 1960s [e.g. 2] and, for some applications,  
 15

16 are still in use today. Glass is retained at the face of the wall system using a me-  
17 chanical clamp. Rubber gaskets permit relative movement, in the plane of the  
18 wall, between the glass and the metal frame. So, the glass does not prevent the  
19 aluminium members from moving laterally. Also, the mechanical clamp at the  
20 edge of the glass permits rotation, as shown in Figure 1-A, so glass deflections  
21 do not cause the framing member to twist about its longitudinal axis.

22 Another means of securing glass to its frame is to use an adhesive. This  
23 approach, known as “structural glazing” and shown in Figure 1-B, is relatively  
24 new. The first high-rise tower with a structurally glazed curtain wall was com-  
25 pleted as recently as 1986 [4, p. 53]. Since then, architects have embraced the  
26 new aesthetic, using the technology to create large, flat facades, without any  
27 metal components to the exterior of the glass. Structural glazing has become a  
28 common and conspicuous feature of large buildings around the world. Current  
29 structural design methods and usage guidelines for the adhesives – structural  
30 silicone sealants – are detailed in ASTM C1401 [5]. The reasons for inclusion of  
31 the “glazing tape” shown in Figures 1-B and 1-D, and the effect that this tape  
32 has upon structural performance, are explained in Section 7.3.

33 Figure 1-B shows the E-shaped male and female extrusions that together  
34 form the split mullion of a modern unitized curtain wall. In such designs, the  
35 facade is made up of discrete panels that can be prefabricated. Because of this,  
36 and other, practical advantages [6 p. 4-5; 7 p. 86], the great majority of the  
37 world’s new curtain wall is of this type [8, p. 82]. From a structural standpoint  
38 however, the split mullion’s narrow profiles are, in torsion, less rigid than the  
39 box sections they replace (Figure 1-A). Consequently, it is frequently the case  
40 that prevention of buckling is the dominant concern for today’s facade engineers.

41 Lateral torsional buckling (LTB) is the mode of structural failure caused and  
42 characterized by extreme axial rotation of a flexural member’s cross section. At  
43 the onset of failure by LTB, a glazing system’s profiles deflect in the manner  
44 shown in part D of Figure 1. The analysis of LTB is complex [e.g. 9, Chap-  
45 ter 5], and is affected by parameters aside from bending moment distribution,  
46 material properties, cross-sectional shape and distance between supports. Other

47 significant particulars are the member's initial straightness, and also the load  
48 eccentricities, which may themselves be functions of the profile's rotation.

49 If one of a member's flanges is restrained to prevent it from rotating about its  
50 long axis, then LTB can be prevented. The moments that are transferred to such  
51 braces can be estimated analytically [e.g. 9, Equation 12.10], and the magnitude  
52 of the required torsional resistance is small. In a typical, unitized curtain wall  
53 system, the panes of glass or other sheet infill materials that are connected to  
54 the mullion's outer flanges have ample structural capacity to serve a torsional  
55 braces. However, current design guides advise that, even in structurally glazed  
56 systems, glass and infill materials should not be considered to be restraints  
57 [e.g. 10]. Consequently, in structural analysis, mullions are modelled [as in 11,  
58 Part VIII, pp. 56-61] with the assumption that no moment is imparted to them  
59 by the glass. The structural idealization of the glass support is a hinge, as shown  
60 in Figure 1-C.

61 In reality, because the structural sealant joint has stiffness, Figure 1-D might  
62 better describe a unitized mullion's mid-span condition under wind load. In this  
63 diagram, positive wind pressure causes the glass to deflect toward the interior of  
64 the building and, as a consequence, moment is transferred through the structural  
65 silicone sealant to the mullion profiles, whose inner flanges move toward each  
66 other. The onset of LTB in the mullion profiles will, therefore, be affected by  
67 the moment resistance of the sealant joint.

68 Facade engineers are interested in improving current methods of predicting  
69 LTB [12, 13] because, with continuing advances in the sizes of the panes that  
70 can be processed by glass fabricators, the structural members in exterior wall  
71 systems are becoming increasingly slender [10]. Research by others [e.g. 14]  
72 suggests that a structural silicone joint may provide sufficient support to pre-  
73 vent LTB in some cases, but a recent survey [12] showed that facade design  
74 professionals have insufficient information to assess whether an attachment to a  
75 glazing system's frame will be effective as an LTB restraint. The analytical steps  
76 proposed in this present paper might therefore be incorporated in a more com-  
77 prehensive model, to predict the angle through which a framing extrusion will

78 rotate when full design load is applied, and thus demonstrate that the frame's  
79 resistance to LTB is adequate.

80 Intuitively, it might seem dangerous to create structures using metal flexural  
81 members that remain stable only because they are supported by restraints made  
82 of glass. Glass is, after all, a brittle material, and building facades must be de-  
83 signed with the expectation that occasional breakages will occur. It is therefore  
84 worth explaining that the governing design loads acting upon a building's facade  
85 are usually wind pressures. So, if breakage destroys a pane, it is true that its  
86 frame will no longer be restrained by the glass but, at the same time, the frame  
87 will no longer receive wind load. Therefore, failure of the glass will not cause a  
88 failure of the metal structure that it restrains.

89 With greater understanding of the joint's behaviour and with a more sophis-  
90 ticated structural model, it may be possible to reduce the mass of metal required  
91 to construct a curtain wall. The opportunity for metal savings exists because,  
92 in the design of modern mullion extrusion shapes, it is common that stability  
93 – in particular, resistance to lateral torsional buckling – is the governing struc-  
94 tural design consideration. If structural sealant joints can be shown to provide  
95 effective lateral or torsional restraint for their frames, then facade engineers will  
96 be able to make use of lighter profiles [e.g. 14]. The pursuit of efficient curtain  
97 wall design solutions is worthwhile, not only because of the cost savings that  
98 can be attained by reducing material usage, but also because, amongst common  
99 building materials, the embodied energy in aluminium is unusually high [15,  
100 p.74] and so significant environmental benefit can be achieved by controlling  
101 metal content [16].

102 The manner in which a mullion profile might be caused to rotate about  
103 its lengthwise axis is illustrated in Figure 1-D. When the magnitude of this  
104 rotation is sufficiently large then, aside from any structural consequences, other  
105 functions of the wall can be affected. For example, it is possible that the interior  
106 flanges of the male and female profiles will disengage, breaching the weather  
107 seal. Curtain wall system failures of this sort, caused by excessive rotation of a  
108 member about its extrusion axis, could be predicted during the design process

109 if facade engineers were provided with a model of the relationship between  
110 moment and rotation in a structural silicone joint. For these two reasons –  
111 firstly to help curtain wall designers determine whether a particular structural  
112 sealant connection can provide torsional bracing for a mullion, and secondly to  
113 quantify the axial moment transmitted – the objective of the research described  
114 in this paper has been to develop a simple algebraic method to describe the  
115 rotational stiffness of a structural sealant joint, and to collect experimental  
116 data with which to validate the mathematical model.

117 The terms “elastic modulus”, “Young’s modulus” and “modulus of elastic-  
118 ity” are equivalent, and may be used interchangeably. For a sealant, the pub-  
119 lished value of this property is usually that measured 14 days [e.g. 17] or 21 days  
120 [18] after creation of the sample. Research [17, p.967] has, however, revealed  
121 that the Young’s modulus of a particular structural silicone sealant, DC-995,  
122 can rise dramatically during the 100 days following the assessment on day 14.  
123 In that single-component sealant – one that does not need to be mixed with a  
124 separate catalyst prior to application – the increase in elastic modulus “was in  
125 the range of 850-950 %”. If the results of this study are to be applied in practice  
126 then there is a need to understand the changes in Young’s modulus that occur  
127 as a sealant ages. Therefore, the rotational stiffness of a two-component sealant,  
128 DC-983 – a type that is commonly used when structurally glazed curtain wall  
129 panels are prefabricated in a factory – has been assessed at 14, 114 and 214  
130 days. Also, each sample’s indentation hardness was measured at 214 days.

131 Apart from the rubber pads used in vibration-absorbing mountings, elas-  
132 tomeric materials are rarely encountered in building structures, and it may  
133 therefore be helpful to summarize their special properties. Structural silicone  
134 sealants are viscoelastic, meaning that an applied load causes damped elastic  
135 deflection, and so the magnitude of stress depends not just upon the magnitude  
136 of strain, but also upon the rate of change in strain. Figure 2, shows the rela-  
137 tionship between tensile stress and strain [19, Table 1] for the particular sealant  
138 that has been tested in this study, DC-983. It can be seen that, even when  
139 strain is increased at a constant rate, in accordance with ASTM C1135 [18],

140 the material's behaviour is not linear-elastic. If, however, the product is used  
 141 within the allowable range defined by the manufacturer, so that strain does not  
 142 exceed 25 %, then a linear-elastic idealization results in a maximum error of less  
 143 than 9 %.

144 While considering the precision with which a sealant's elasticity can be mod-  
 145 elled, it should be noted that the expected level of variability in laboratory mea-  
 146 surements is high. If a sealant's stress is measured twice, at 10 % tensile strain,  
 147 using the ASTM C1135 method, there is 95 % probability that the two measure-  
 148 ments will differ by less than 0.041 MPa (6 lbf/in<sup>2</sup>) if the tests are carried out  
 149 in the same laboratory, or by 0.090 MPa (13 lbf/in<sup>2</sup>) if carried out in different  
 150 laboratories [18, Table 1]. For the DC-983 sealant tested in this present study,  
 151 these 95 % probability ranges are, respectively, equivalent to 20.7 % and 44.8 %  
 152 of the published value of stress at 10 % strain, which is 0.2 MPa [20].

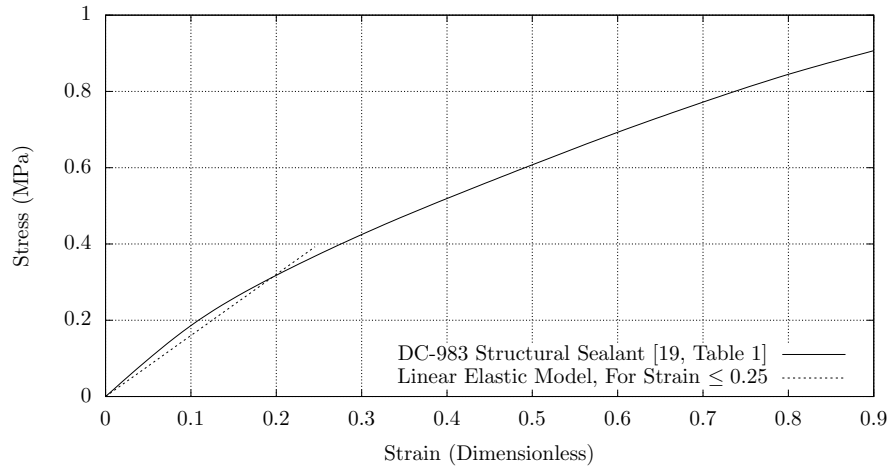


Figure 2: Stress with respect to strain in DC-983 structural sealant, measured by the ASTM C1135 laboratory method [18]. Also plotted is a linear idealization, for the useable range defined by the sealant manufacturer, in which strain is limited to 25 %.

## 153 2. Algebraic Model of Moment Resistance

154 In the model that is commonly used by practising facade engineers to as-  
 155 sess the load capacity of a structural sealant joint [5, Section 30], it is assumed

156 that the glass remains flat when wind pressure is applied, and that the sealant  
 157 experiences only tensile or only compressive stress. Several researchers [e.g. 21]  
 158 have carried out sealant analyses that take glass deflection and the sealant’s  
 159 shear stresses into account. In these more sophisticated studies, solutions for  
 160 particular design conditions have been obtained numerically, using finite differ-  
 161 ence or finite element techniques. While the results obtained in this way are  
 162 comprehensive – the entire stress field is revealed – the process of preparing  
 163 numerical models is time consuming, making it impractical to use this approach  
 164 to investigate the many and varied design cases that might be encountered in  
 165 a real building’s facade. It has therefore been this present study’s aim to find,  
 166 and to validate experimentally, a set of simple, closed-form algebraic expressions  
 167 that may, in the future, be incorporated in a design code.

168 For the sake of simplicity, here the assumption will be made that structural  
 169 sealants obey Hooke’s law. The validity of this approach is discussed later,  
 170 in Section 7.1. Adopting a linear-elastic model makes it possible to consider  
 171 separately the different components of load, and to sum their effects using su-  
 172 perposition. The application of a pure moment causes a unit length of sealant  
 173 joint to deform elastically from its original rectangular cross section into a trape-  
 174 zoid, as shown in Figure 3, then the force in the equivalent couple,  $F$ , can be  
 175 expressed in terms of the sealant’s Young’s modulus,  $E_{ss}$ . Considering either  
 176 side of the sealant joint – the area in compression or the area in tension – the  
 177 mean stress is half of the extreme fiber stress. Also, recalling that the force re-  
 178 quired to extend a linear-elastic material is the product of cross sectional area,  
 179 strain and elastic modulus:

$$F = \frac{B\Delta g E_{ss}}{4g}, \quad (1)$$

180 where  $B$  is the “bite” or width of the adhesive plane,  $g$  is the “glueline” or sealant  
 181 thickness, and  $\Delta g$  is the maximum distance through which the sealant extends.  
 182 Similarly, the sum total moment per unit length of sealant joint,  $M$ , can be  
 183 obtained by integrating torque over the width of the triangular compression



184

and tension zones that have been shaded in Figure 3:

$$M = \frac{2E_{ss}}{g} \int_{x=0}^{\frac{B}{2}} \frac{2x^2 \Delta g}{B} dx, \quad (2)$$

185

if the  $x$ -axis is horizontal in the right hand diagram of Figure 3. Hence:

$$M = \frac{B^2 \Delta g E_{ss}}{6g}. \quad (3)$$

186

If the eccentricity of  $F$  from the joint's centreline is  $Q$  then  $M = 2FQ$ . Sub-

187

stituting for  $F$  and  $M$  from Equations 1 and 3 gives the value of  $Q$ , which is

188

$B/3$ . This is, plainly, the standard result for a triangular load zone, in which

189

the amplitude of force varies linearly with distance.

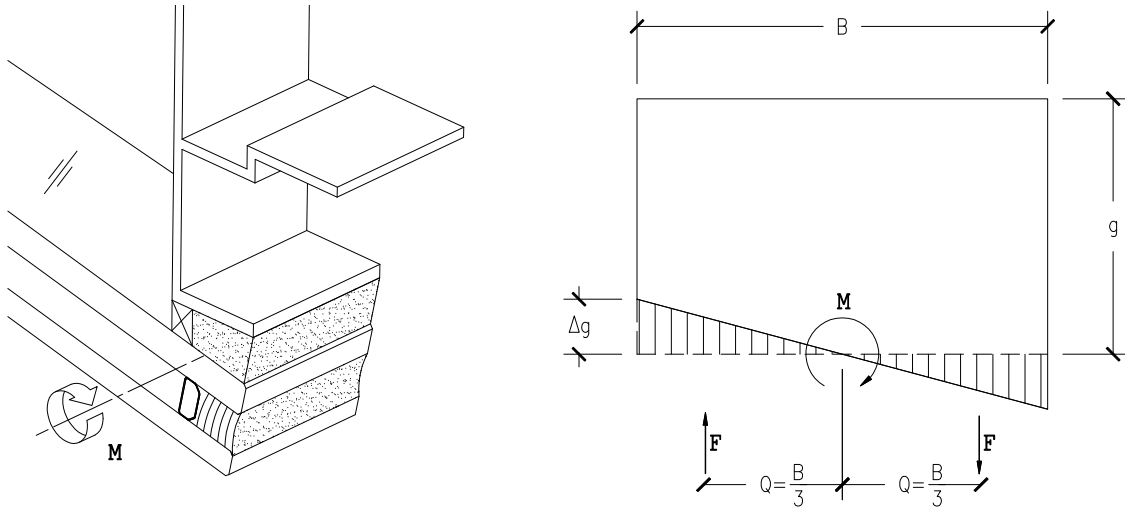


Figure 3: The edges of a glass pane rotate (*Left*) under the action of wind pressure. A section through the loaded structural sealant joint (*Right*) shows its trapezoidal shape.

190

If the angle through which the glass edge rotates is  $\alpha$  then, from Figure 3,

191

$\tan \alpha = 2\Delta g/B$ . These rotations are small – usually only a few degrees – and so

192

$\alpha$  is a close approximation to  $\tan \alpha$ , when  $\alpha$  is measured in radians. This small

193

angle assumption is reasonable while  $\alpha$  is less than 0.176 radians (10 degrees).

194

In this range,  $\alpha = 2\Delta g/B$ , and Equation 3 can be rewritten:

$$M = \alpha \frac{B^3 E_{ss}}{12g}. \quad (4)$$

195

### 3. A More Sophisticated Model of Moment Resistance

Wolf and Cleland-Host [22] used a polynomial expressions to describe relationship between stress and strain in two-part structural silicone sealants. Their coefficients, below, were chosen to fit the experimentally determined responses of two commercial products, A and B, that had been tested at 22°C after one year of aging. For a given strain,  $\varepsilon$ , the corresponding stress,  $f$ , was found to be:

$$f_A(\varepsilon) = 0.87244\varepsilon^5 - 1.74222\varepsilon^4 + 1.59336\varepsilon^3 - 1.17958\varepsilon^2 + 1.01308\varepsilon \quad (5)$$

$$f_B(\varepsilon) = 3.80874\varepsilon^5 - 7.37014\varepsilon^4 + 4.44015\varepsilon^3 - 1.02037\varepsilon^2 + 0.93614\varepsilon \quad (6)$$

196

These two stress-strain curves are plotted in Figure 4.

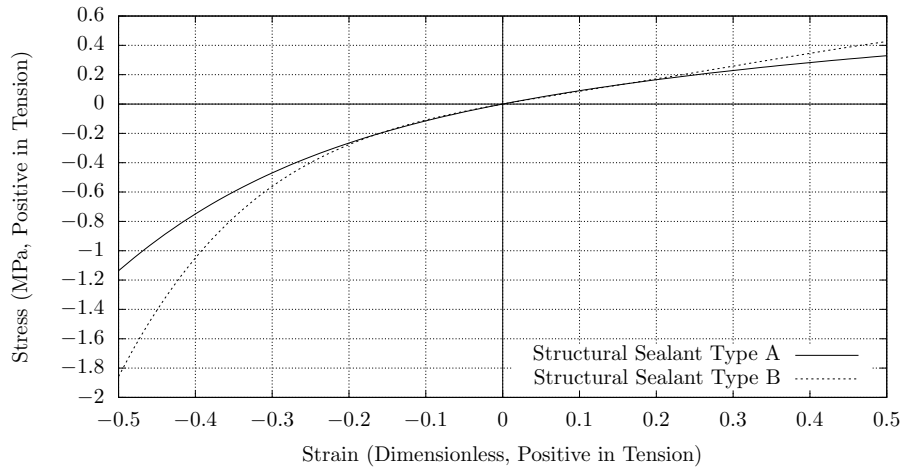


Figure 4: Curves chosen by Wolf and Cleland-Host [22, Table 2] to fit experimental measurements of stress and strain in two different two-part structural silicone sealants.

197

The market names of the sealant products tested by Wolf and Cleland-Host were not revealed, and so it cannot be assumed that their elastic properties

198

199 will match those of the sealant tested in this study, or those of the sealant  
 200 used in a given glazing system. However, in Figure 4 it can be seen that the  
 201 sealants' elastic moduli are greater in compression than they are in tension, and  
 202 in this discussion the presumption is that such asymmetry is typical amongst all  
 203 structural silicone sealants. A further supposition is that the stress-strain curve  
 204 for any particular structural glazing sealant, or a reasonable approximation to  
 205 it, can be obtained by applying a constant scaling factor to the stress function  
 206 in Equation 5 or 6. Expressed another way, for a sealant Z:

$$f_Z(\varepsilon) \simeq k_Z f_A(\varepsilon), \quad (7)$$

207 where  $k_Z$  is a constant.

208 While formulating the previous rotational stiffness model, described in Sec-  
 209 tion 2, the stress-strain curve from a tensile test was examined, and it was argued  
 210 that, within the range between zero and 25 % strain, a linear-elastic approxima-  
 211 tion is sufficiently accurate for engineering design purposes. A constant value  
 212 of Young's modulus was then assumed to apply in the sealant joint's tension  
 213 zone, and also in the compression zone. Because of its simplicity, that previous  
 214 model still may be of interest to engineers, but, in reality, Young's modulus is  
 215 a function of strain, and is greater in compression than in tension. Therefore,  
 216 when a pure moment is applied about the axis of a sealant joint, it will deflect  
 217 in the manner sketched in Figure 5.

218 In order to determine the joint's rotational stiffness, a first step is to develop  
 219 an expression for the width of the tension zone,  $l$ . Because the joint is in static  
 220 equilibrium, the total tensile force is equal to the total compressive force, so:

$$0 = \int_{x=-(B-l)}^l f\left(\frac{x}{l} \frac{\Delta g}{g}\right) dx. \quad (8)$$

221 The result may be used to determine  $l$ , and then the total moment for a given

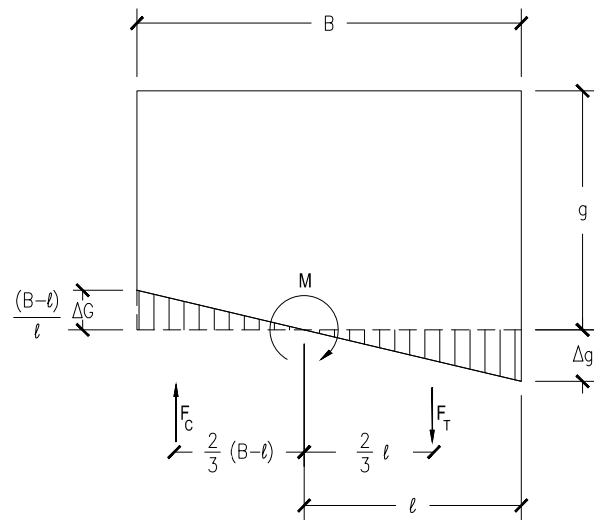


Figure 5: Cross section through structural sealant deflecting solely because of a moment about the joint's axis, with asymmetric tension and compression zones (cf. Figure 3). The positions of equivalent concentrated forces are based on the premise that Young's modulus is constant in the tension zone and constant in the compression zone.

222

$\Delta g$  can be found by integration:

$$M = \int_{x=-(B-l)}^l x f \left( \frac{x}{l} \frac{\Delta g}{g} \right) dx. \quad (9)$$

223

224

225

226

227

When the sealant's stress-strain curve is given in polynomial form, as in Equation 5, mathematical integration is easy. However, the results cannot readily be reduced to a simple closed-form algebraic formula relating rotation to moment. What is needed is an approximation that can be expressed simply, and which is, at the same time, less crude than the model proposed in Section 2.

228

229

230

231

232

233

In the analysis that follows, it is assumed that a constant modulus of elasticity,  $E_{ss}$ , applies throughout the tension zone, and that its value is independent of strain. It is also assumed that the modulus of elasticity within the region that is in compression,  $E_C$ , is constant for any given angle of joint rotation, but it's value increases with rotation. The applicability of this set of assumptions is discussed in Section 7.1.

234

235

236

237

238

Applying these new premises to the sealant joint shown in Figure 5, the equivalent concentrated force in the triangular tension zone,  $F_T$ , and in the triangular compression zone,  $F_C$ , can be found in the same way that they were found for Equation 1. Static equilibrium is achieved when  $F_T + F_C = 0$ , hence:

$$\frac{l}{2} \frac{\Delta g}{g} E_{ss} + \frac{-(B-l)}{2} \frac{(B-l)}{l} \frac{\Delta g}{g} E_C = 0, \quad (10)$$

239

which reduces to:

$$\frac{E_{ss}}{E_C} = \frac{(B-l)^2}{l^2}. \quad (11)$$

240

241

By definition, if  $\varepsilon$  is a tensile strain, and if  $f$  is a stress function similar to Equation 5 or 6:

$$E_{ss} = \frac{f(\varepsilon)}{\varepsilon}. \quad (12)$$

242

The strains on the compression side are smaller in magnitude than those on the

243

tension side, and  $\varepsilon$  is a tensile strain, so:

$$E_C = \frac{-f\left(\frac{(B-l)}{l}\varepsilon\right)}{\frac{(B-l)}{l}\varepsilon}. \quad (13)$$

244

Substituting the above two expressions, for  $E_{ss}$  and  $E_C$  in Equation 11, and simplifying:

245

$$f(\varepsilon) = -f\left(\frac{-(B-l)}{l}\varepsilon\right)\frac{(B-l)}{l}. \quad (14)$$

246

The way in which the width of the tensile zone varies with strain has been determined numerically, using Equation 14, and the results are presented in Figure 6. The graph shows that, at the limit of allowable strain, when  $\Delta g/g = 0.25$ , which is the condition that will be of greatest interest to designers,  $(B-l)/l \simeq 0.78$ , which is to say that  $l \simeq 0.56B$ .

247

248

249

250

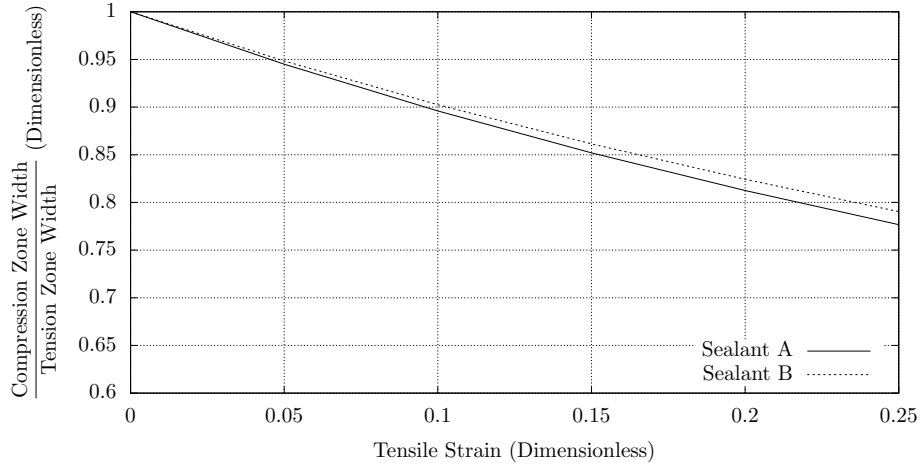


Figure 6: Width of the compression zone, as a proportion of the width of the tension zone, in a structural sealant joint subject to axial moment. Using the variable names shown in Figure 5, this is  $(B-l)/l$ .

251

The modified versions of Equations 1 and 3, for force and moment, are:

$$F_T = -F_C = \frac{l}{2} \frac{\Delta g}{g} E_{ss} \quad (15)$$

252 and,

$$M = \frac{Bl}{3} \frac{\Delta g}{g} E_{ss}. \quad (16)$$

253 When the glass edge rotation is  $\alpha$  then, from Figure 5,  $\alpha = \Delta g/l$ , where  $\alpha$   
254 is less than 0.176 radians. Equation 16 now can be rewritten:

$$M = \alpha \frac{Bl^2 E_{ss}}{3g}. \quad (17)$$

#### 255 4. Experimental Method & Results

256 Three identical samples of structural silicone sealant were prepared specifi-  
257 cally for this study. In each sample, DC-983 sealant was applied between two  
258 painted aluminium extrusions, to create a joint in which the thickness of the  
259 joint or “glueline”,  $g$ , was 6 mm. The sealant joint was orientated with its axis  
260 perpendicular to the axis of the extrusions, as shown in Figure 7: the width  
261 of the contact surface between the sealant and the painted metal substrate or  
262 “bite”,  $B$ , was 24.2 mm, and the joint’s length was 110 mm. The glazing tape,  
263 seen in Figure 7, was not removed: it remained in place throughout the test  
264 process.

265 The thickness of the metal in the extruded aluminium box sections was  
266 sufficiently great – approximately 7 mm – that the magnitude of deflections  
267 occurring within the metal parts during testing was negligible.

268 DC-983 is available in two colors, gray and black, and the two varieties have  
269 different physical properties [20]. The samples used in this study were black.

270 After the sealant samples had been created, and during the periods between  
271 tests, they were stored in a covered outdoor location where they were not ex-  
272 posed to rain or direct sunlight. There, the ambient temperature varied between  
273 20°C and 36°C, and the relative humidity ranged from 65% to 85%. Commen-  
274 tary in Section 6 considers the effect that environmental conditions have upon  
275 the sealant’s physical properties.

276 For each test, one of the sample’s two extrusions was clamped to a rigid  
277 support as indicated in Figure 7. A counterbalance was positioned so that the

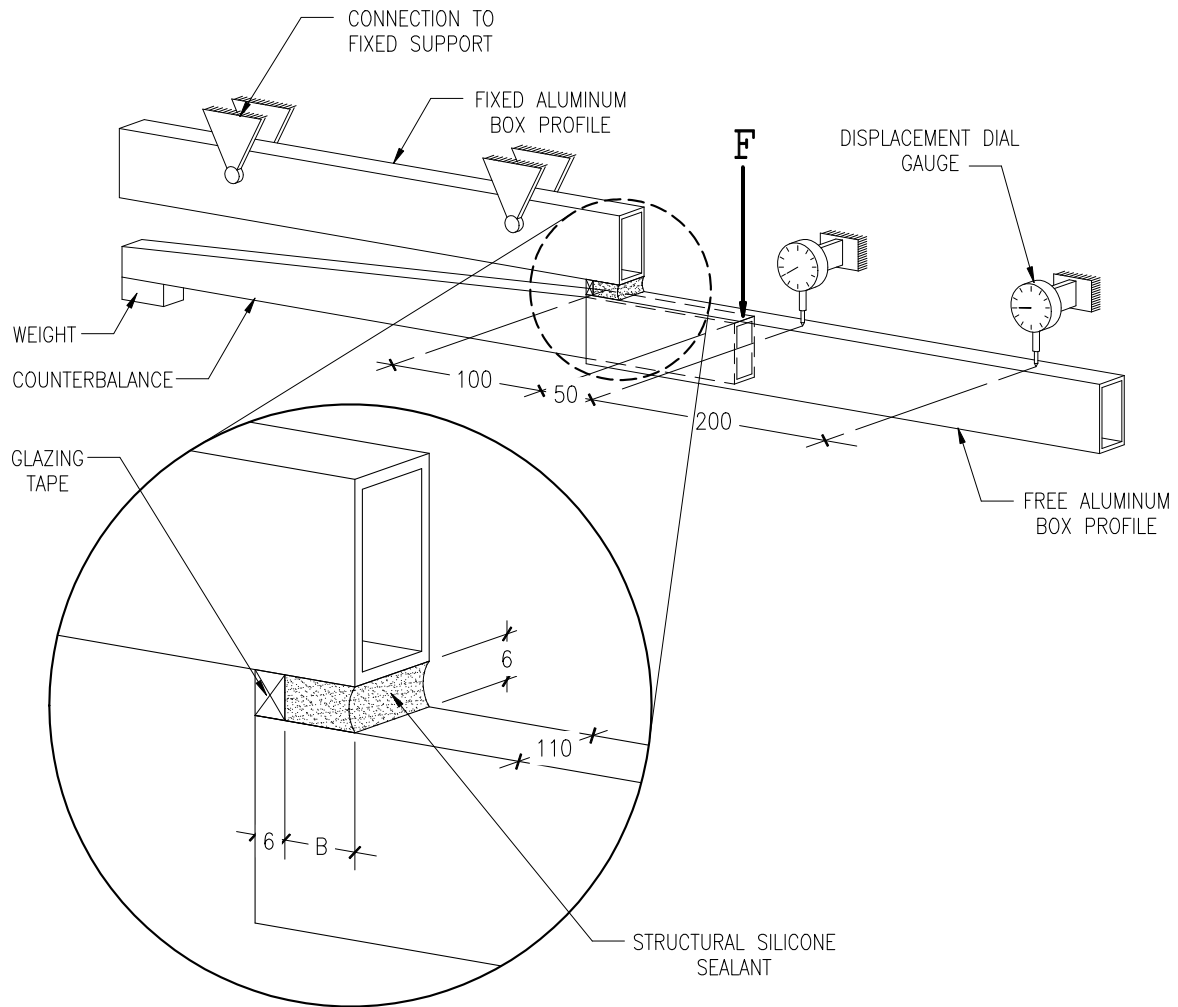


Figure 7: Experimental apparatus used to measure rotation of structural sealant joint with respect to applied moment. The box section on the left is rigidly fixed, while that on the right is supported only by the structural sealant sample. Load  $F$  is applied to the free side, while deflection is measured using dial gauges.

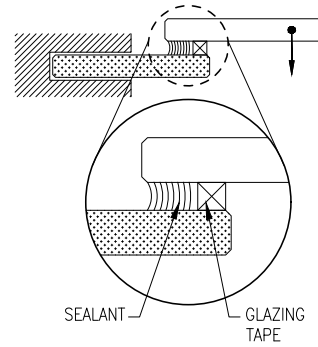
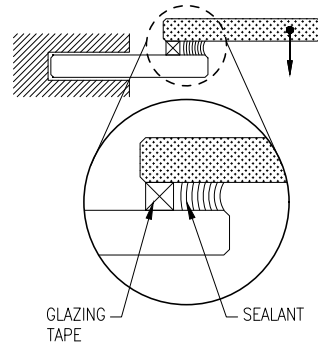


278 axis of the suspended extrusion, which was supported only by the structural  
279 silicone joint, was also horizontal. The load, which varied as a function of time,  
280 was applied to the suspended extrusion, at a distance of 100 mm from the sealant  
281 joint's centreline. Force was increased by 3.2 N every 30 seconds until the free  
282 beam's deflection was near to the maximum that the instruments could measure,  
283 or until the strain in the sealant was near to the 25 % limit established by the  
284 sealant's manufacturer [20]. Thereafter, force was removed incrementally, at the  
285 same rate as it had been applied. Immediately prior to each change in load,  
286 the position of the moving side of the sample was measured using dial gauges,  
287 graduated in hundredths of a millimeter, located as shown in Figure 7.

288 Each of the three sealant specimens was held and loaded, in sequence, in four  
289 different orientations, as shown in Table 1. Therefore, on each of the occasions  
290 that the samples' properties were measured – after 14, 114 and 214 days – the  
291 test procedure described above was carried out twelve times in total.

292 Figure 8 shows the magnitude of rotation about the axis of the sealant joint,  
293 plotted against applied moment, for two example sets of data – test numbers  
294 9 and 10. The readings presented are those recorded while the load was being  
295 increased and while the load was being reduced. The hysteresis patterns are  
296 typical of those seen in the other test results.

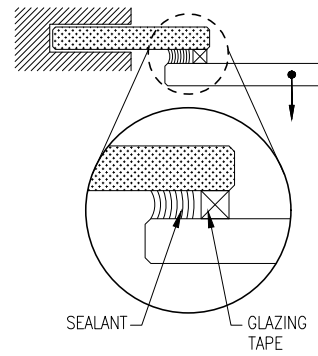
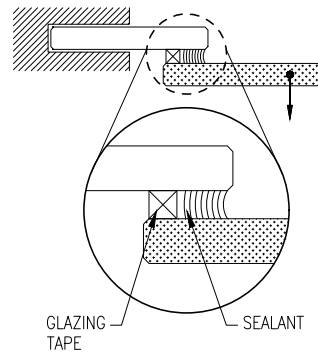
297 The measurements plotted in Figure 9-A are similar – rotation with respect  
298 to moment – but records of all 12 tests carried out on the fourteenth day are  
299 presented. For clarity, the part of each sample's response that has been plotted  
300 is that recorded during the initial phase of the test, while the applied load was  
301 increasing. Figure 9-B is the mean tensile stress, averaged over the sealant  
302 joint's contact area, caused by the applied load together with the dead load of  
303 the suspended part of the test sample and its counterbalance. At any given  
304 test load, the magnitude of this direct stress is much less than the stress caused  
305 by the applied moment. The graph showing direct stress, Figure 9-B, has been  
306 provided beneath the rotation-moment plot so that the description of stresses is  
307 complete. This information may be of interest because, even though this paper's  
308 models presume that the relationship between stress and strain is linear, it is



Simulating positive  
wind pressure.

Sample 1, Test 1  
Sample 2, Test 5  
Sample 3, Test 9

Sample 1, Test 4  
Sample 2, Test 7  
Sample 3, Test 11



Simulating negative  
wind pressure.

Sample 1, Test 2  
Sample 2, Test 6  
Sample 3, Test 10

Sample 1, Test 3  
Sample 2, Test 8  
Sample 3, Test 12

Table 1: In a series of twelve tests, each of the three sealant specimens was tested in four different orientations. To make it easier to differentiate the two box sections, one has been drawn with shading. The enlarged views show the position of glazing tape in the joint.

309 known [22] that the elasticity of a structural sealant does, in reality, vary with  
310 stress.

311 When the sample's fixed beam was positioned below its free beam, which  
312 was the case during tests 1, 4, 5, 7, 9 and 11 (see Table 1), the counterbalance  
313 was not of the same length and mass as that used during the other tests. Hence,  
314 the absolute magnitudes of mean tensile or compressive stresses in the sealant  
315 during tests 1, 4, 5, 7, 9 and 11 were lower than those during other tests.

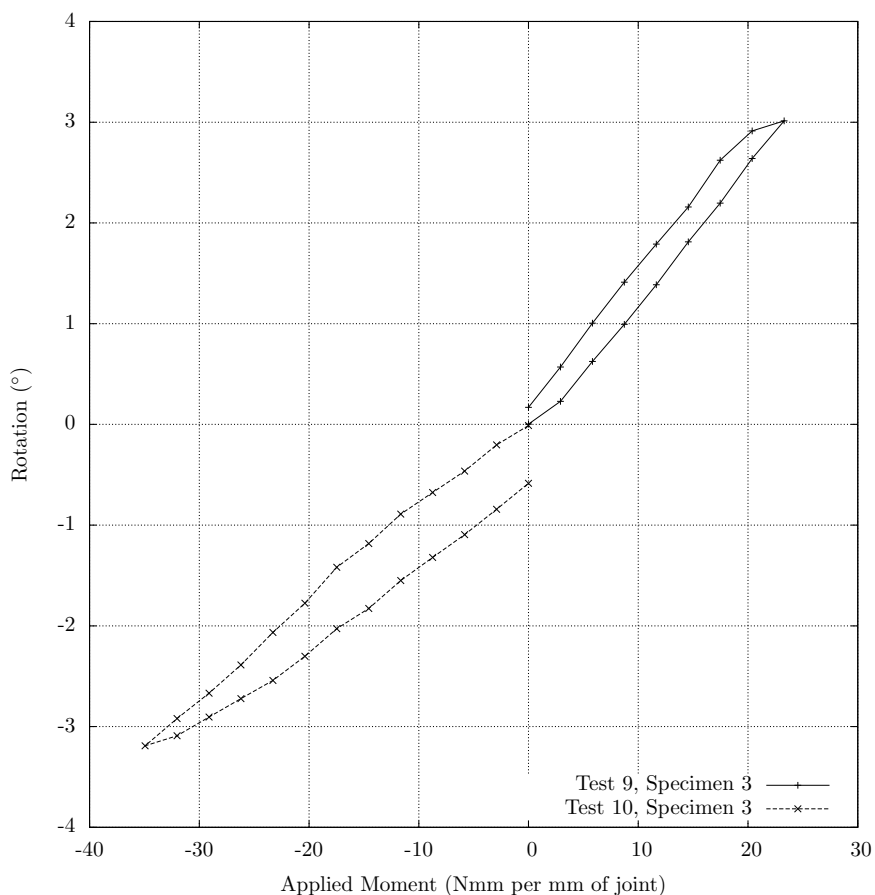


Figure 8: Rotation, as a function of the moment applied during tests 9 and 10, fourteen days after creation of the sealant samples.

316 The sequence of tests was repeated one hundred days later, on day 114, and  
317 then repeated again after a further one hundred days, on day 214. These two

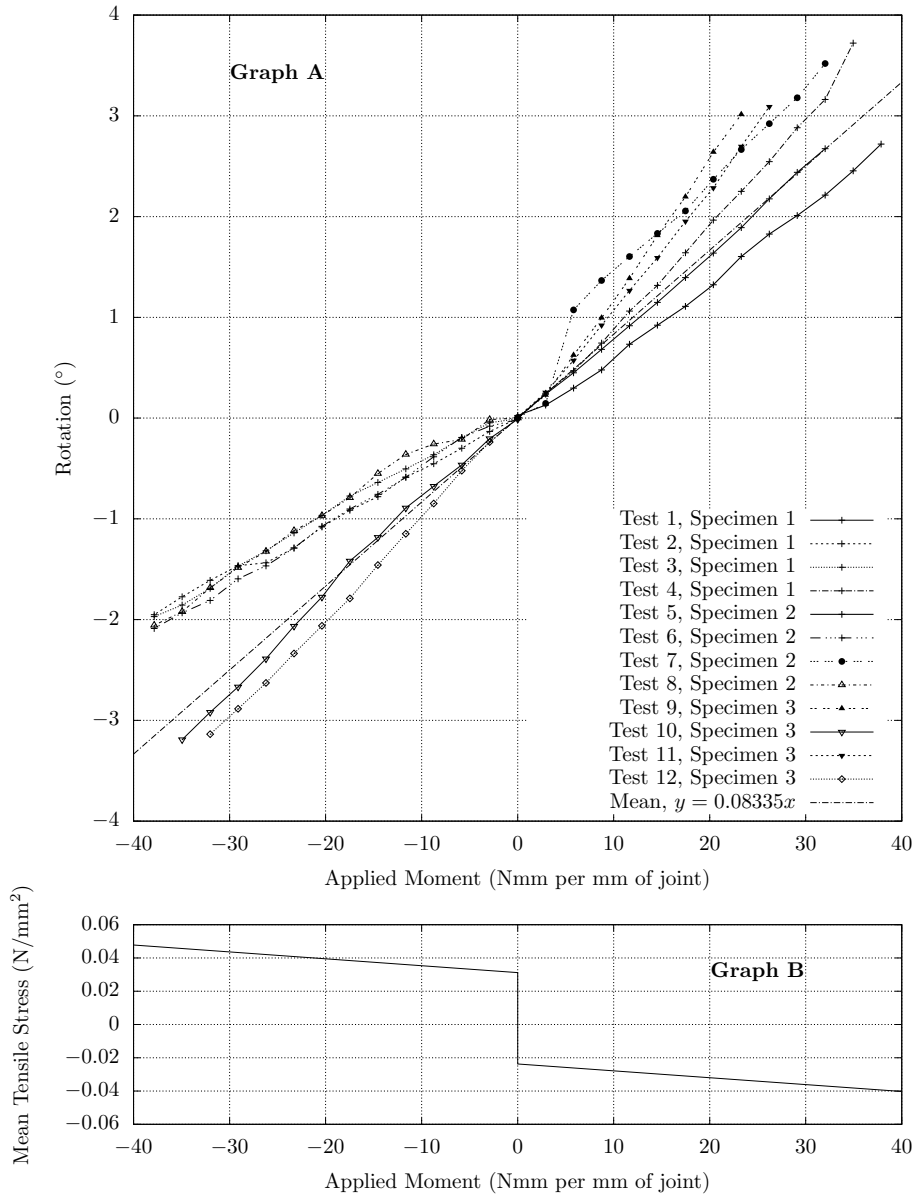


Figure 9: (Graph A) Rotation with respect to applied moment, measured 14 days after creation of the sealant joint, for each of the twelve test cases. (Graph B) Mean direct stress, averaged over the sealant-to-substrate surface area.

318 sets of rotation measurements, plotted against applied moment, are shown in  
319 Figures 10-A and 11-A respectively. For completeness, the corresponding direct  
320 stresses are given in Figures 10-B and 11-B.

321 In summary, the torsional resistance of sealant joints has been measured in  
322 the laboratory. Each of three specimens was tested in four different orientations,  
323 as shown in Table 1, after 14, 114 and 214 days. All 36 measured rotational  
324 stiffness are presented, in the form of a histogram, in Figure 12.

## 325 5. Young's Modulus of Structural Silicone Sealant

326 After rotational resistance had been measured for the third time, on day  
327 214, each specimen was partially disassembled by separating the sealant from  
328 one of its metal substrates using a sharp blade. At the newly-exposed surfaces  
329 of sealant and glazing tape, hardness was found using a Shore A indentation  
330 tester [23, 24]. For each of the three specimens, sealant hardness measurements  
331 were taken at six locations. For specimens 1 and 2, glazing tape hardness  
332 measurements were taken at six locations. As the glazing tape in specimen 3  
333 had been damaged when it was separated from its substrate, it was possible  
334 to measure its hardness in only one location. Minimum, mean and maximum  
335 values are shown in Table 2. Because the thickness of material tested was equal  
336 to the sealant joint's glueline, 6 mm, it was not necessary to apply any correction  
337 to the gauge readings [25, Figure 3]. As the glazing tape is narrow – only 6 mm  
338 in width – the centre of the tip of the indentation tester could not be positioned  
339 more than 3 mm from the tape's edge. The close proximity of the indenter  
340 to the edge is likely to have influenced the measurements but, as discussed in  
341 Section 7.3, the tape's properties are not considered in this paper's algebraic  
342 models of sealant joint behaviour.

343 The behaviour of an elastic material under the tip of a hardness instrument's  
344 indenter was considered by Gent [26], who proposed the following theoretical

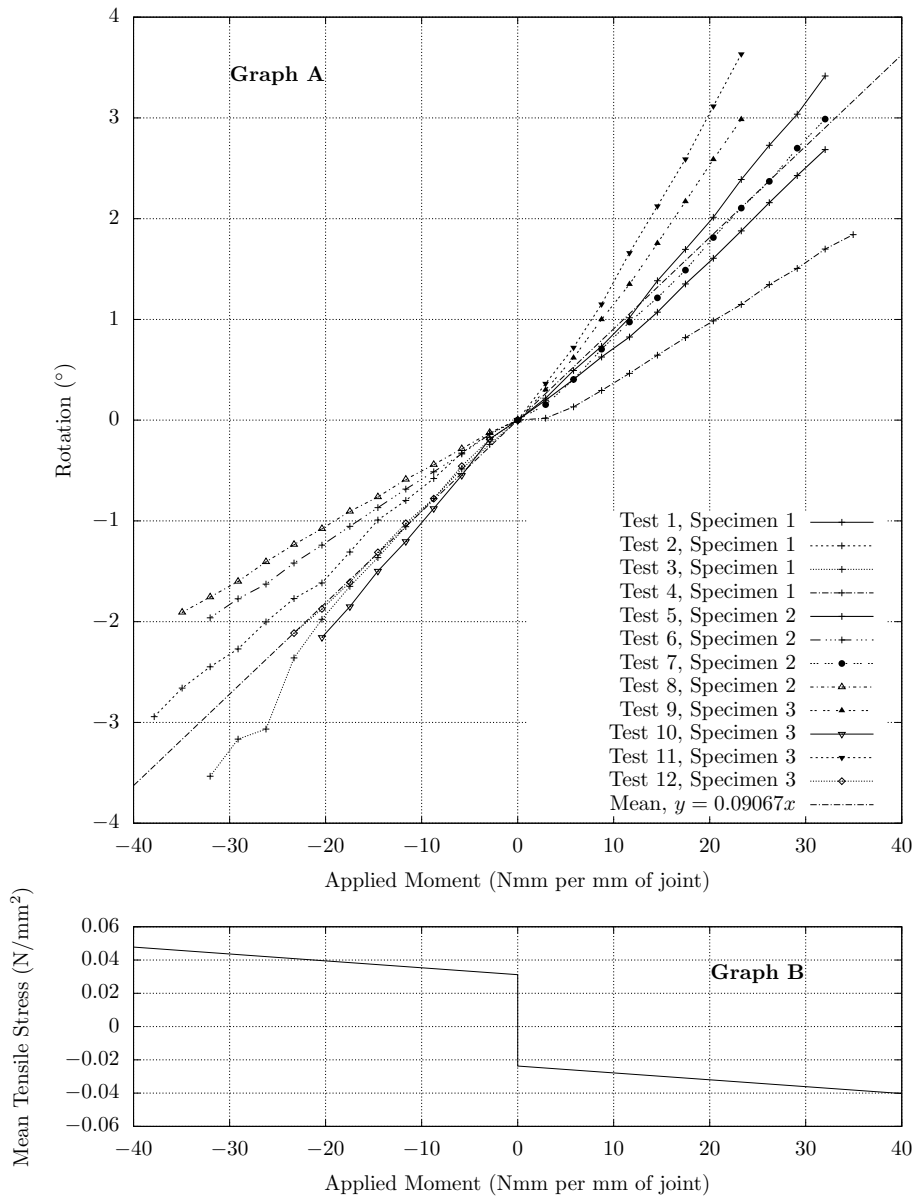


Figure 10: (Graph A) Rotation with respect to applied moment, measured 114 days after creation of the sealant joint, for each of the twelve test cases. (Graph B) Mean stress, averaged over the sealant-to-substrate surface area.

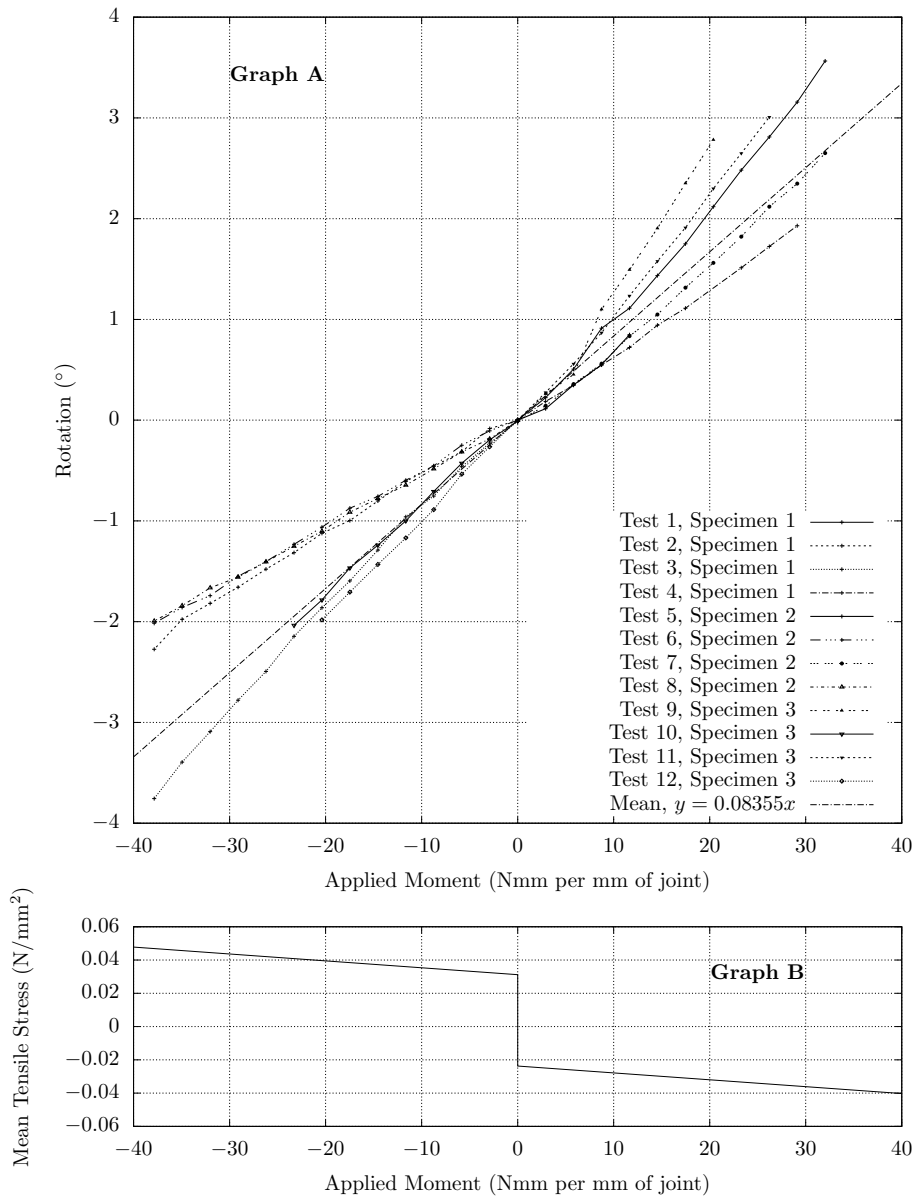


Figure 11: (Graph A) Rotation with respect to applied moment, measured 214 days after creation of the sealant joint, for each of the twelve test cases. (Graph B) Mean stress, averaged over the sealant-to-substrate surface area.

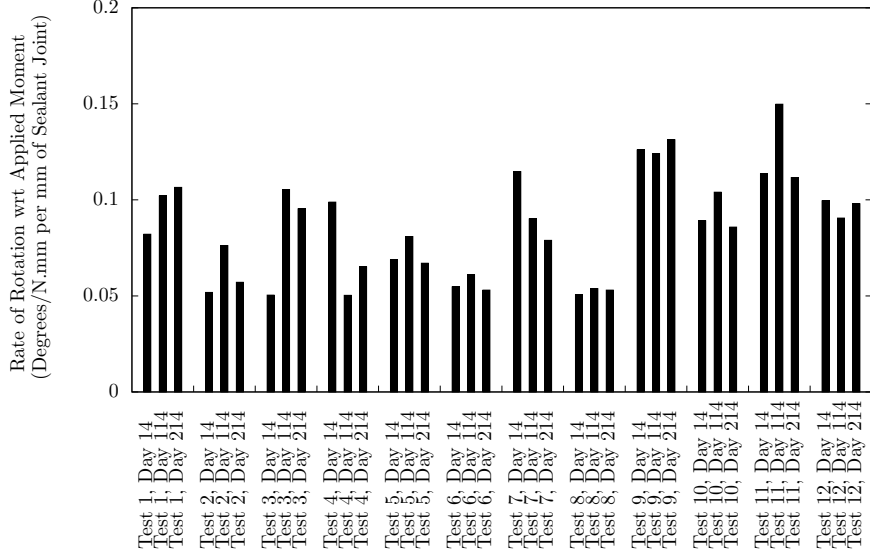


Figure 12: The torsional resistances of three structural silicone sealant specimens, were measured in four different orientations (Table 1), after 14, 114 and 214 days. The experimental results are presented in this histogram. Rotational stiffnesses are the gradients of straight lines fitted to the test results shown in Figures 9, 10 and 11, and the units are degrees of rotation per N.mm of applied moment, per mm of axial length of sealant joint.

Material Tested	Specimen Number	Shore A Hardness		
		Min.	Mean	Max.
Structural sealant.	1	34	<b>35.3</b>	38
Structural sealant.	2	32	<b>33.2</b>	34
Structural sealant.	3	34	<b>34.5</b>	36
Glazing tape.	1	30	<b>31.2</b>	35
Glazing tape.	2	21	<b>25.3</b>	28
Glazing tape.	3	32	<b>32.0</b>	32

Table 2: Hardness of the DC-983 structural sealant samples, as well as the hardness of the glazing tape, measured with a Shore A indentation gauge 214 days after creating the specimens.



345 relationship between Young’s modulus,  $E$ , and Shore A hardness,  $S$ ;

$$E = \frac{0.0981(56 + 7.62336S)}{0.137505(254 - 2.54S)}. \quad (18)$$

346 In various studies documented in the existing literature, for a wide range  
347 of different materials, values of Young’s modulus determined by tensile testing  
348 have been compared with values based on indentation hardness measurements.  
349 Regression analysis of the laboratory data [e.g. 27] has shown that, away from  
350 the extreme ends of the hardness scale, the relationship between Young’s mod-  
351 ulus and Shore A hardness is in close agreement with that predicted by Gent  
352 (Equation 18). There is however significant scatter in the experimental data,  
353 and for this reason values of Young’s modulus derived from individual indenta-  
354 tion hardness measurements should be considered to be indicative rather than  
355 precise.

356 According to the manufacturer’s technical data sheet [20], the hardness of  
357 the sealant used in this study, DC-983, should be in the range between 35 and  
358 45 on the Shore A scale. Gent’s conversion method, Equation 18, implies that  
359 the Young’s modulus will be in the range between 1.39 and 2.03 MPa.

360 The different estimated values for the Young’s modulus of the DC-983 sealant  
361 samples tested in this study, obtained by the methods outlined in this section,  
362 are summarized in Table 3.

## 363 **6. Discussion of Experimental Findings**

364 It is known that the apparent elasticity of a viscoelastic material varies with  
365 the magnitude of strain, strain rate and the direction of loading [for structural  
366 sealant, see 22], and it is therefore to be expected that any quantification of  
367 Young’s modulus will be influenced by the manner in which measurement is  
368 made. In Table 3, the values of Young’s modulus in the second and third  
369 rows have been obtained from tensile tests, those in the first and last rows are  
370 based on indentation hardness measurements, while the estimates in the fourth  
371 and fifth rows are those implied by the rotational stiffness equations that were

Basis for Estimate	Age	Shore A Hardness			Implied Young's Modulus		
	Days	Min.	Mean	Max.	Min. N/mm <sup>2</sup>	Mean N/mm <sup>2</sup>	Max. N/mm <sup>2</sup>
Sealant manufacturer's published Shore A range [20], converted to Young's modulus using Equation 18.	7	35	-	45	1.39	<b>1.71</b>	2.03
Young's modulus implied by sealant manufacturer's published stress at 10 % strain [20].	21	-	-	-	-	<b>2.00</b>	-
Linear elastic model based on laboratory tension measurements [19] at up to 25 % strain (Figure 2).	21	-	-	-	-	<b>1.60</b>	-
Mean measured joint stiffness (Figures 9, 10 & 11) converted to Young's modulus using Equation 4.	14	-	-	-	2.31	<b>3.49</b>	5.77
	114	-	-	-	1.94	<b>3.21</b>	5.79
	214	-	-	-	2.22	<b>3.48</b>	5.49
Mean measured joint stiffness (Figures 9, 10 & 11) converted to Young's modulus using Equation 17.	14	-	-	-	1.83	<b>2.76</b>	4.56
	114	-	-	-	1.54	<b>2.54</b>	4.57
	214	-	-	-	1.75	<b>2.75</b>	4.34
Measured Shore A hardness (mean of values in Table 2) converted to Young's modulus using Equation 18.	214	32	34.3	38	1.24	<b>1.36</b>	1.57

Table 3: Different estimated values of Young's modulus for the DC-983 structural silicone samples tested in this study.

372 developed in Sections 2 and 3. Therefore it is true that, here, apples have not  
373 been compared with apples. However, the following observations can be made:

- 374 (a) The behavioural model that underlies the estimates in the fourth row of  
375 Table 3, that is the basis for Equations 3 and 4, assumes that the relationship  
376 between stress and strain is the same whether the sealant is in tension or  
377 compression. The result of this simplification – that is to say, ignoring the  
378 increase in elastic modulus that occurs when the sealant is in compression  
379 – is an increase in the sealant’s apparent elastic modulus in tension.
- 380 (b) Taking laboratory measurements of rotation with respect to moment, and  
381 finding the elastic moduli that are implied by the asymmetric tension-  
382 compression model that is the basis for Equation 16, leads to the val-  
383 ues shown in the fifth row. The mean of these implied elastic moduli is  
384  $2.68 \text{ N/mm}^2$ , which is, in comparison to the elastic moduli obtained using  
385 Equations 3 and 4, closer to the value published by sealant manufacturer  
386 ( $2.00 \text{ N/mm}^2$ , in the second row of Table 3).

387 As noted previously, the sealant samples were cured, stored, and tested in  
388 conditions ranging between  $20^\circ\text{C}$  and  $36^\circ\text{C}$ , and 65 % to 85 % relative humidity.  
389 This environment was therefore warmer and more humid than the reference  
390 conditions – a constant  $25^\circ\text{C}$  and 50 % relative humidity – in which the sealant  
391 manufacturer’s own test specimens cured [20]. The manufacturer indicates [also  
392 20] that elevated temperatures do increase the rate of curing, but published  
393 test results [28, Table 1] suggest that the impact of the non-standard storage  
394 temperature and humidity upon the modulus of elasticity of this particular  
395 sealant, DC-983, is small. Also, it should be remembered that any deviation  
396 from the ideal laboratory conditions has been modest in comparison with the  
397 extremes that are experienced by structural sealants in service, where facade  
398 surface temperatures of  $-20^\circ\text{C}$  through  $+80^\circ\text{C}$  can be encountered.

399

## 7. Validity of the Mathematical Model

400

401

402

403

404

The rotation of an idealized structural sealant joint can be predicted using Equation 3. In this model, the relationship between stress and strain in the sealant is linear, and the glazing tape, shown in Figures 1-B, 1-D and 7, does not affect the moment resistance. It is worth revisiting these two premises in the light of the experimental findings.

405

### *7.1. Variability of the Sealant's Apparent Modulus of Elasticity*

406

407

408

409

410

411

412

413

414

415

416

417

418

The algebraic model presented in Section 2 is based upon the assumption that structural sealant obeys Hooke's law. However, it has been noted already that actual stresses, measured in conditions of steadily increasing strain, differ from the linear-elastic ideal by around 9% in the range of strain between zero and 25%. Further deviation from the theoretical model is to be expected in service, where, in wind storms, the rate of change in pressure or the duration of load application might differ greatly from this study's conditions. In addition, the material's elastic modulus may be influenced by its cyclic loading history [29]. In short, a structural designer should be aware that the effective value of a structural sealant's Young's modulus may vary with factors such as age, temperature and loading history, and the range may be a large proportion of the mean. This is not to say, however, that a structural sealant cannot function effectively as a restraint for the metal member to which it is bonded.

419

420

421

422

423

424

425

426

427

428

The mathematical representations of rotational resistance are based upon premises that are not perfectly consistent with each other. For example, in Section 3, the modulus of elasticity on the compressed side of joint is assumed to vary with glass rotation but, at the same time, it is assumed that elasticity at any given angle of rotation is constant within the triangular compression zone, even though strain varies in that region. There is therefore an element of arbitrariness in the formulation of the models. Rather than try to correct the inconsistencies or to create a more realistic and more complex model, a more practical approach might be to use an empirical constant to adjust the crude relationships, such as Equation 3, offered in Section 2.

429 *7.2. Influence of Sealant Joint's Cross Sectional Aspect Ratio*

430 Normally, when a piece of incompressible or partially compressible solid is  
431 stretched in one direction, there is a reduction in the area of its cross section  
432 in the perpendicular plane. This, of course, is Poisson's effect. However, when  
433 sealant is bonded to a rigid substrate then, in the material adjacent to the  
434 contact surface, Poisson's stresses are resisted by the adhesive connection. Be-  
435 cause changes in cross-sectional shape are inhibited in this way, in vicinity of  
436 the substrate, the sealant's effective elasticity is reduced. Changing the shape  
437 of a sealant joint therefore effects the material's apparent rigidity,  $E_r$ . As the  
438 ratio of bite to glueline or, using the variable names shown in Figures 3 and 5,  
439  $B/g$ , increases, so the sealant's apparent rigidity will increase.

440 The value of a sealant's elastic modulus that is published by the product's  
441 manufacturer is, commonly, determined by the ASTM C1135 method [18], using  
442 sealant specimens with a bite to glueline ratio of 1:1. Laboratory tests have  
443 shown [30, p. 42] that changing the joint's aspect ratio from 1:1 to 2:1 "more than  
444 doubles" the apparent modulus of elasticity in a tensile test. Recently Descamps,  
445 Hayez and Chabih [31] studied the influence that aspect ratio has upon the  
446 rigidity of a particular, two-part, structural silicone sealant, DC-993, and they  
447 concluded that the relationship is described by the second order polynomial  
448 below;

$$E_r = \left[ 0.1506 \left( \frac{B}{g} \right)^2 + 0.3409 \frac{B}{g} + 1.0852 \right] E. \quad (19)$$

449 The expressions for a sealant joint's moment resistance, which were developed  
450 in Sections 2 and 3, can be modified to model the significance of joint shape  
451 by replacing Young's modulus,  $E$ , with the effective rigidity of the sealant,  $E_r$ ,  
452 from Equation 19.

453 The modulus of elasticity of the structural sealant used in this present  
454 study's laboratory tests, DC-983, is similar to that of the product considered by  
455 Descamps et al. According to the technical data published by the manufacturer  
456 [32], the Shore A hardness of DC-993, measured after 7 days at 25°C and 50%  
457 relative humidity, is 40, while that of the DC-983 [20] tested in this investigation

458 is in the range between 35 and 45. It might appear, therefore, that Equation 19  
459 could be applied to this current analysis. However, if the sealant’s modulus  
460 of elasticity is in the range between 1.36 and 2.0 MPa (see Table 3), then the  
461 modulus of rigidity of the joints tested in the laboratory (Section 4) will, from  
462 Equation 19, be in the range from 6.68 to 9.8 MPa. This range is well above  
463 the mean apparent value implied by the rotational stiffness test measurements,  
464 which is less than 3.5/,MPa (Table 3, row 4).

465 It remains reasonable to argue that the apparent modulus of elasticity based  
466 on torsional rigidity measurement is greater than the modulus of elasticity in-  
467 ferred from indentation hardness measurements because the sealant joint sam-  
468 ples have a high bite to glueline ratio. However, Equation 19 was developed by  
469 Descamps and coauthors for the analysis of structural sealant joints in tension,  
470 and it appears to overestimate the rigidity of joint in which, as in this instance,  
471 the predominant load is torsion.

### 472 *7.3. The Influence of Glazing Tape*

473 The “glazing tape” adjacent to the sealant in the test specimens (see Fig-  
474 ures 1-D & 7) is an open-cell foam spacer, square in cross-section, with acrylic  
475 adhesive on the two sides in contact with the substrates. Its purpose is to  
476 maintain the required distance between the bonding surfaces while the sealant  
477 is being applied and while it is curing but, as is the usual practice in glazing  
478 systems, the tape was not subsequently removed from the joint.

479 In the proposed mathematical models for the joint’s rotational stiffness, es-  
480 tablished in Sections 2 and 3, the glazing tape has been ignored. When the load  
481 applied to the test specimens caused tension in the sealant beside the glazing  
482 tape – during tests 3, 8 and 12 (see diagram in Table 1) – it was obvious from  
483 inspection that the tape’s adhesive held it to only one side of the joint, and the  
484 tape therefore played no part in the transfer of moment. This condition is out-  
485 lined in the left hand diagram of Figure 13. Conversely, during tests 4, 7 and 11,  
486 the glazing tape was placed in compression, in the manner shown in the right  
487 side of Figure 13. However, the test results do not show a consistent increase

488 in the joint's rotational stiffness. The experimental data therefore support the  
 489 assumption that the contribution of glazing tape can be ignored in analysis of  
 490 moment resistance.

491 In some glazing systems, the material used to separate the metal and glass  
 492 may be much harder than the glazing tape that has been used in this study.  
 493 When such a separator is placed in compression, the deflected shape of the  
 494 sealant joint will be similar to that shown in right hand diagram of Figure 13,  
 495 except that the fulcrum for glass rotation might be at, or near to, the upper  
 496 right hand corner of the sealant's initial, unloaded cross section. Here, all of the  
 497 sealant is in placed in tension, and the joint's theoretical moment resistance can  
 498 be determined using the expression below, which has been derived in the same  
 499 way as Equation 4:

$$E_{ss} = \frac{3gM}{\alpha B^3}. \quad (20)$$

## 500 8. Quantifying Axial Moment in Framing Members

501 When a rectangular pane of glass is simply supported at its perimeter and  
 502 subjected to a uniform pressure acting normal to its plane, the deflected shape

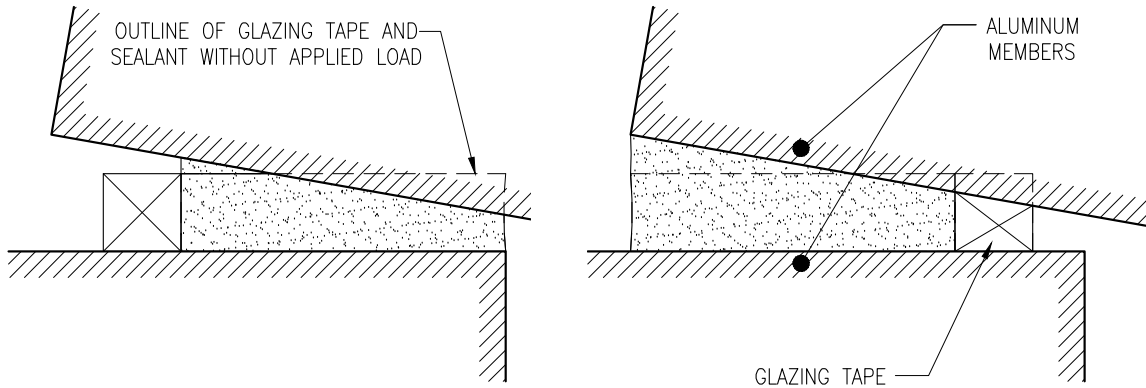


Figure 13: Glazing tape separates from one of its substrates when the adjacent sealant is in tension (Left). However, when the adjacent sealant is compressed (Right), the glazing tape is also placed in compression.

503 of its surface, measured along any line parallel to an edge, is similar to one half  
 504 period of a sinusoid [33, Equation 36] if the sides of the pane are not greatly  
 505 different in length. It is to be noted that this approach will under-estimate edge  
 506 rotations away from the centre of the sides of plates with higher aspect ratios  
 507 [34, Figures 56-71]. This point is best explained with reference to Figure 14,  
 508 which shows the actual deflected shape of a rectangular plate with aspect ratio  
 509 of three, and that shape's deviation from the sinusoidal idealization. At any  
 510 point along the centreline parallel to the long sides, other than at the plate's  
 511 geometric centre, the actual deflection exceeds the sinusoidal model's prediction.

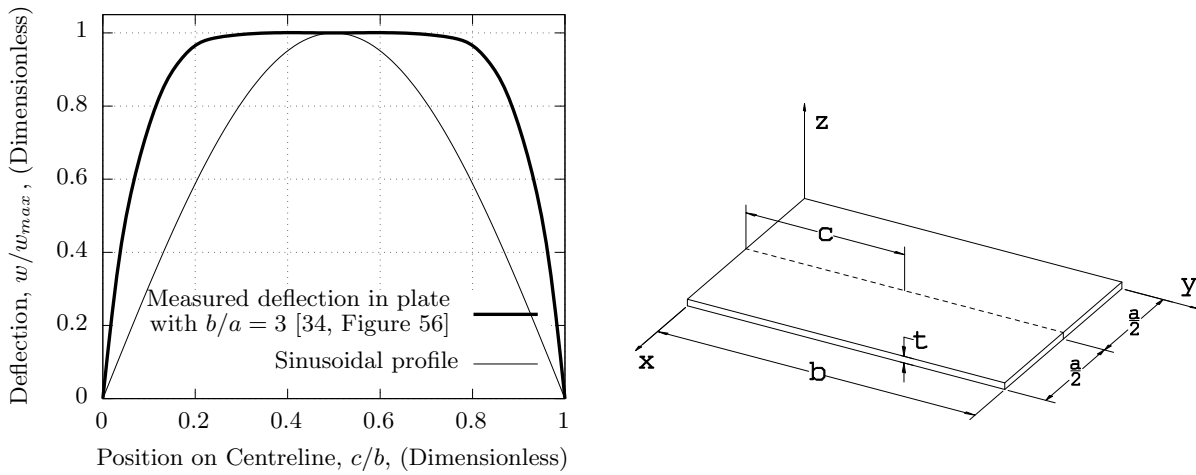


Figure 14: The graph's heavy line shows the deflected shape of an initially-flat rectangular plate with aspect ratio  $b/a = 3$ , measured at the centreline parallel to the long sides, when a uniform pressure is applied to the plate's surface [traced from 34, Figure 56].

512 Even though the actual rotations at both the long and the short edges of a  
 513 rectangular plate will, if the plate's edges are disparate in size, be larger than  
 514 those predicted by the sinusoidal surface model, the model is still useful because  
 515 its mathematical description is simple. If the lengths of a panes' short and long  
 516 sides are, respectively,  $a$  in the  $x$  direction and  $b$  in the  $y$  direction, if  $w_c$  is the  
 517 central deflection, and if  $w_{x,y}$  is the deflection at point  $(x, y)$ , then an expression



518 for the sinusoidal surface is;

$$w_{x,y} = w_c \sin\left(\frac{\pi x}{a}\right) \sin\left(\frac{\pi y}{b}\right). \quad (21)$$

519 The gradient in the  $x$ -direction is obtained by differentiating partially;

$$\frac{\partial w_{x,y}}{\partial x} = \frac{\pi w_c}{a} \cos\left(\frac{\pi x}{a}\right) \sin\left(\frac{\pi y}{b}\right). \quad (22)$$

520 so, at the middle of the pane's longer side, where  $x = 0$  and  $y = b/2$ ;

$$\frac{\partial w_{x,y}}{\partial x} = \frac{\pi w_c}{a}. \quad (23)$$

521 As is evident in the diagram at the right hand side of Figure 3, the gradient  
522 of the glass surface at the sealant joint is  $2\Delta g/B$ . Substituting for gradient in  
523 Equation 23 gives;

$$\Delta g = \frac{\pi B w_c}{2a}. \quad (24)$$

524 In reality, when wind pressure acts upon a structurally glazed pane, the  
525 sealant at its perimeter experiences both a direct force and a moment. However,  
526 it is easiest to convey the relative importance of these two components of load  
527 if the force is considered to act, as shown in Figure 15, through an imaginary  
528 lever attached to the frame, at a distance  $e$  from the centreline of the sealant  
529 joint. The significance of a given eccentricity will be immediately apparent to  
530 curtain wall designers, who are accustomed to seeing similar lever arms in the  
531 shapes of brackets used to connect Mullions to a building's primary structure.

532 In a structurally optimized design, the width of the sealant bite will be  
533 minimized so that the actual tensile stress is equal to the maximum allowable  
534 stress,  $F_t$ . So, considering a unit length of sealant joint and substituting for  $M$   
535 in Equation 3;

$$F_t B e = \frac{B^2 \Delta g E_{ss}}{6g}, \quad (25)$$

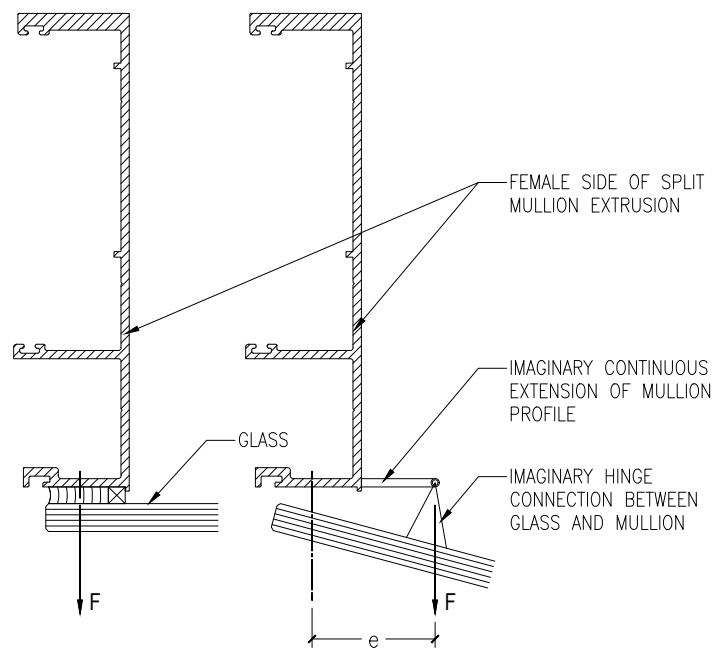


Figure 15: The current analytical convention is that loads transferred from glass to mullion are considered to act through the centre of the structural sealant (*Left*), but in reality, because rotation occurs at the glass edge (*Right*), there is an effective eccentricity,  $e$ , between the force and the sealant joint.

536

then substituting for  $\Delta g$  from Equation 24, and simplifying;

$$e = \frac{\pi B^2 E_{ss} w_c}{12 F_t a g}. \quad (26)$$

537

538

539

540

541

In practice, the maximum allowable glass deflection is often specified as a proportion of the length of the pane's shorter side. A limit commonly found in design codes and technical specifications for glazing – for example, the Australian design code for glass in buildings [35, Section 3.3.3] – is  $w_c = a/60$ . At this deflection condition, Equation 26 becomes;

$$e = \frac{\pi B^2 E_{ss}}{720 F_t g}. \quad (27)$$

542

543

544

545

546

547

548

549

550

551

552

553

554

555

556

557

558

Typical numerical values can be assigned to the variables in Equation 27 in order to assess whether the magnitude of the turning moment – that imparted by the glass, through the structural sealant, to the glazing system's metal frame – is of practical significance. Assuming that the structural sealant industry's standard tensile stress limit is observed,  $F_t = 139$  kPa [5, Section 27.5], and that the geometry and elastic modulus of the joint are similar to those in the samples that were tested in this study, with glueline  $g = 6$  mm, bite  $B = 22.5$  mm, and  $E_{ss} = 4.0$  MPa (see Table 3), then the eccentricity of the load,  $e$ , measured from the joint's centreline, is 10.6 mm. The effect of the moment upon the glazing frame will of course depend upon the cross-sectional shape and span of the mullion profile, but it is probable that, in most cases, an eccentricity of this magnitude could safely be neglected by the framing designer. However, if the sealant's elastic modulus were to be at the upper end of the range that has been observed in one-part structural silicones, say  $E_{ss} = 20.0$  MPa [e.g. 17, Figure 6], then the value of  $e$  would be 53.0 mm. Such a large eccentricity certainly would concern the designer of a typical unitized curtain wall system with open, E-shaped mullion extrusions.

559

## 9. Conclusions

560

When wind load causes the glass or other sheet infill material at the face of a structurally glazed curtain wall to deflect, moments are induced about the longitudinal axes of the framing members.

561

562

563

Using the analytical methods proposed in this paper, facade engineers can incorporate mathematical expressions – for a sealant joint’s rotational stiffness and, hence, for axial moment – in their structural models of curtain wall mullions. There are at least two practical incentives to do so. Firstly, it will be possible to identify, during the design process, cases in which excessive axial rotation of a proposed mullion extrusion would impair its non-structural functions, such as the effectiveness of its air seals. Secondly, if analysis shows that the torsional restraint provided by a sealant-to-glass connection is sufficient to prevent lateral torsional buckling, then there will be an opportunity to create framing members containing less aluminium than would be needed if the established structural design conventions were to be observed. For this second application, however, further research into the stability of structurally glazed members will be needed to demonstrate that they can be reliably restrained by structural sealant in the all of the conditions that might be experienced by the facades of real buildings.

564

565

566

567

568

569

570

571

572

573

574

575

576

577

578

Data sets have been obtained by physical testing and the results show that, for any one sample sealant joint, the relationship between rotation and applied moment is practically linear. The variation between one sample and another is, however, considerable: in a population of sealant joints, one standard deviation is approximately one third of the mean value. So, when estimating the magnitude of the moment transferred to the frame of a structurally glazed pane, a pragmatic approach will be to consider a range of values for the sealant joint’s stiffness. When establishing that range, it should be kept in mind that the variability in rotational stiffness of structural sealant joints in a real building’s curtain wall panels will, because of normal batch-to-batch inconsistencies in the sealant properties, dimensional tolerances, differences in loading history

579

580

581

582

583

584

585

586

587

588

589 and other factors, be greater than that observed in these tests, which have been  
590 carried out in relatively tightly controlled conditions.

591 The hardness of this study's sealant samples, measured by the indentation  
592 method (Table 3, last row), was found to lie within the range published by  
593 the sealant manufacturer (Table 3, first row). However, the mean value of  
594 this study's laboratory measurements of rotational stiffness, when used with  
595 the simple mathematical model proposed in Section 2, suggests that the elastic  
596 modulus of the sealant samples (Table 3, fourth row) is approximately 70 %  
597 greater than the value published by the sealant manufacturer (Table 3, second  
598 row). The more refined behavioural model, laid out in Section 3, which acknowl-  
599 edges a difference between the sealant's properties in tension and compression,  
600 also leads to a value of Young's modulus that is an apparent overestimate: the  
601 computed value (Table 3, fifth row) is about 34 % greater than that indicated  
602 by the sealant manufacturer (Table 3, second row). Nonetheless, even if pre-  
603 dictions of rotational stiffness based upon this paper's algebraic models are not  
604 in precise agreement with the laboratory results, the models are still useful to  
605 facade designers. Providing the analysis of an adhesive joint's rotational stiff-  
606 ness will take into consideration a suitably wide range of possible values for the  
607 structural sealant's elastic modulus, some degree of inaccuracy in the predictive  
608 model will not be of consequence.

609 Others [17] have recorded a manyfold increase in the Young's modulus of  
610 single-part structural silicone sealant, occurring during the months after the  
611 initial fortnight of curing. The DC-983 two-part sealant specimens prepared  
612 for this investigation were tested at 14, 114 and 214 days, but no significant  
613 change in modulus was observed. This observation shows that, at 14 days, the  
614 cross-linking of polymer chains within the sealant – the curing process – was  
615 complete or substantially complete.

616 Using the formulae that have been presented in this paper, designers of  
617 curtain wall systems will be able to estimate quickly, without a requirement for  
618 numerical modelling, load eccentricities that are ignored in standard structural  
619 analyses. The information will be of greatest interest when the metal framing

620 members to which structural glazing is to be applied are susceptible to rotation  
621 about their longitudinal axes – for example, if unsupported spans are long, and  
622 if the profiles have low torsional rigidity.

## 623 **10. Acknowledgements**

624 The authors are grateful to Mr. James Chant, Chairman of Seapac Philip-  
625 pines Inc., who provided the material samples used in these tests. Mr. Lawrence  
626 Carbary of Dow Corning reviewed a draft of this paper and made helpful com-  
627 ments. Staff of PTCC Facade Design, led by Engineer Warren Tan and Mr. Rene  
628 Ramiscal helped to commission the test rig and collect data. PTCC’s Mr. Jhun  
629 Fabrero transformed the authors’ hand sketches into CAD drawings.

## 630 **References**

- 631 [1] Yeomans D. The pre-history of the curtain wall 1998;14:59–82. URL:  
632 [http://www.arct.cam.ac.uk/Downloads/chs/final-chs-vol.14/  
633 chs-vol.14-pp.59-to-82.pdf](http://www.arct.cam.ac.uk/Downloads/chs/final-chs-vol.14/chs-vol.14-pp.59-to-82.pdf).
- 634 [2] Ábalos I, Herreros J. Tower and Office: From Modernist Theory to Con-  
635 temporary Practice. MIT Press; 2003. ISBN 0-262-01191-3.
- 636 [3] Yeomans D. The origins of the modern curtain wall. APT Bulletin  
637 2001;32:13–8. URL: <http://www.jstor.org/stable/1504688>. doi:10.  
638 2307/1504688.
- 639 [4] Murray S. Contemporary Curtain Wall Architecture. Princeton Architec-  
640 tural Press; 2009. ISBN 978-1-56898-797-2.
- 641 [5] ASTM C1401. Standard Guide for Structural Silicone Sealant Glazing;  
642 2014. doi:10.1520/C1401-14.
- 643 [6] American Architectural Manufacturers Association. Curtain Wall Design  
644 Guide Manual; 2005.

- 645 [7] Watts A. *Modern Construction Envelopes*. 2 ed.; AMBRA—V; 2014.  
646 ISBN 978-3-99043-559-5.
- 647 [8] Yuanda China Holdings Limited. *Global Offering*; 2011. URL:  
648 [www.hkexnews.hk/listedco/listconews/sehk/2011/0420/02789\\_](http://www.hkexnews.hk/listedco/listconews/sehk/2011/0420/02789_1057382/EWF114.pdf)  
649 [1057382/EWF114.pdf](http://www.hkexnews.hk/listedco/listconews/sehk/2011/0420/02789_1057382/EWF114.pdf); (Document available from Hong Kong Stock  
650 Exchange).
- 651 [9] Ziemaiian RD, editor. *Guide to Stability Design Criteria for Metal Struc-*  
652 *tures*. 6 ed.; John Wiley & Sons; 2010. ISBN 978-0-470-08525-7.
- 653 [10] Center For Window and Cladding Technology. *Technical Update No. 7:*  
654 *Buckling of Curtain Wall Mullions*; 2002.
- 655 [11] Aluminum Association. *Aluminum Design Manual*; 2005.
- 656 [12] Goco LT. *Rationalizing assumptions for evaluating the lateral tor-*  
657 *sional buckling strength of aluminium mullion extrusions by EN1999*  
658 *and AA ADM*. Master's thesis; Bath University, UK; 2017. URL:  
659 [https://www.bath.ac.uk/library/dissertations/index.php?](https://www.bath.ac.uk/library/dissertations/index.php?programme=MSc+Architectural+Engineering%3A+Faade+Engineering)  
660 [programme=MSc+Architectural+Engineering%3A+Faade+Engineering](https://www.bath.ac.uk/library/dissertations/index.php?programme=MSc+Architectural+Engineering%3A+Faade+Engineering).
- 661 [13] Skejić D, Lukić M, Buljan N, Vido H. Lateral torsional buckling of split  
662 aluminium mullion. *Key Engineering Materials* 2016;710:445–50. doi:10.  
663 4028/www.scientific.net/KEM.710.445.
- 664 [14] Clift CD, Austin WJ. Lateral buckling in curtain wall systems. *Jour-*  
665 *nal of Structural Engineering* 1989;115(10):2481–95. doi:10.1061/(ASCE)  
666 0733-9445(1989)115:10(2481).
- 667 [15] Hammond G, Jones C. *Embodied Carbon: The Inventory of Carbon and*  
668 *Energy (ICE)*. Bath University and BSRIA; 2011. ISBN 978 0 86022 703  
669 8.
- 670 [16] Lee AD, Shepherd P, Evernden MC, Metcalfe D. *Optimizing the architec-*  
671 *tural layouts and technical specifications of curtain walls to minimize use*

- 672 of aluminium. Structures 2017;13:8–25. doi:10.1016/j.istruc.2017.10.  
673 004.
- 674 [17] Ramesh K, Tock RW, Narayan RS, Vallabhan CVG. Property evaluation  
675 of silicone elastomers used in tension-adhesion joints. Materials and Science  
676 Letters 1995;14:964–7. doi:10.1007/bf02427478.
- 677 [18] ASTM C1135. Standard Test Method for Determining Tensile Adhesion  
678 Properties of Structural Sealants; 2015. doi:10.1520/C1135-15.
- 679 [19] Kimberlain J, Carbary L, Clift CD, Hutley P. Advanced structural silicone  
680 glazing. International Journal of High-Rise Buildings 2013;2(4):345–54.
- 681 [20] Dow Corning Corporation. Product Information: Dow Corning 983  
682 Structural Glazing Sealant; 2012. URL: [http://www.dowcorning.com/  
683 content/publishedlit/63-1110.pdf](http://www.dowcorning.com/content/publishedlit/63-1110.pdf); Dow Corning Form Number: 63-  
684 1110C-01.
- 685 [21] Vallabhan CVG, Aşık MZ. Analysis of structural glazing systems. Comput-  
686 ers and Structures 1997;65:231–9. doi:10.1016/S0045-7949(96)00284-2.
- 687 [22] Wolf AT, Cleland-Host HL. Material properties for use in FEA modeling:  
688 Sealant behaviour with ambient laboratory climate aging. Journal of ASTM  
689 International 2004;1(7):372–84. doi:10.1520/JAI11603.
- 690 [23] ASTM C661. Standard Test Method for Indentation Hardness of  
691 Elastomeric-Type Sealants by Means of a Durometer; 2011. doi:10.1520/  
692 C0661-06R11.
- 693 [24] ASTM D2240. Standard Test Method for Rubber Property – Durometer  
694 Hardness; 2005. doi:10.1520/D2240-05R10.
- 695 [25] Casa L, Mendichi R. Shore A hardness and thickness. Polymer Testing  
696 1986;7:165–75. doi:10.1016/0142-9418(87)90030-4.



- 697 [26] Gent AN. On the relation between indentation hardness and Young's mod-  
698 ulus. *Rubber Chemistry and Technology* 1958;31(4):896–906. doi:10.5254/  
699 1.3542351.
- 700 [27] Larson K. Can You Estimate Modulus From Durometer Hardness  
701 for Silicones?; 2016. URL: [http://www.dowcorning.com/content/  
702 publishedlit/11-3716-01\\_durometer-hardness-for-silicones.pdf](http://www.dowcorning.com/content/publishedlit/11-3716-01_durometer-hardness-for-silicones.pdf);  
703 Dow Corning Form Number: 11-3716-01.
- 704 [28] Tock RW. Temperature and moisture effects on the engineering properties  
705 of silicone sealants. In: O'Connor TF, editor. *Building Sealants: Materi-  
706 als, Properties and Performance*. ASTM STP 1069. American Society for  
707 Testing and Materials; 1990, p. 167–73. doi:10.1520/STP26803S.
- 708 [29] Mullins L. Effect of stretching on the properties of rubber. *Journal of*  
709 *Rubber Research* 1947;16(12):275–89.
- 710 [30] Schmidt CM, Schoenherr WJ, Carbary LD, Takish MS. Performance prop-  
711 erties of silicone structural adhesives. In: Parise CJ, editor. *Science and*  
712 *Technology of Glazing Systems*. American Society for Testing and Materi-  
713 als; 1989, p. 22–45. doi:10.1520/STP22987S.
- 714 [31] Descamps P, Hayez V, Chabih M. Next generation calculation method  
715 for structural silicone joint dimensioning. *Glass Structures & Engineering*  
716 2017;2:169–82. doi:10.1007/s40940-017-0044-7.
- 717 [32] Dow Corning Corporation. Product Information: Dow Corning 993  
718 Structural Glazing Sealant; 2011. URL: [http://www.dowcorning.com/  
719 content/publishedlit/62-0918.pdf](http://www.dowcorning.com/content/publishedlit/62-0918.pdf); Dow Corning Form Number: 62-  
720 0918L-01.
- 721 [33] Wang D, El-Sheikh AI. Large deflection mathematical analysis of rectan-  
722 gular plates. *Journal of Engineering Mechanics* 2005;131:809–21. doi:10.  
723 1061/(ASCE)0733-9399(2005)131:8(809).

- 724 [34] Head RN, Sechler EE. Normal Pressure Tests on Unstiffened  
725 Flat Plates; 1944. URL: [https://ntrs.nasa.gov/search.jsp?R=](https://ntrs.nasa.gov/search.jsp?R=19930086088)  
726 [19930086088](https://ntrs.nasa.gov/search.jsp?R=19930086088); NACA Technical Note 943.
- 727 [35] AS 1288. Glass in Buildings – Selection and Installation; 2006. URL:  
728 <http://www.standards.org.au>.